Chapter 5

Future Research

5.1   Introduction

This chapter describes future research that can improve the current hybrid method and extend it to fracture studies in anisotropic crystals. Section 5.2 details improvements to the current method that can reduce the error sources from the optics, from the analysis method, and from some basic CGS assumptions. Section 5.3 describes the practical requirements for extending this method to anisotropic crystals and demonstrates the need for further analysis by a preliminary investigation of using the current hybrid method for stresses in a ferroelectric crystal, barium titanate.

5.2   Improvements to Experimental Method

5.2.1   Optics

The rotational misalignments of the polarization optics have a significant impact on both the CGS and photoelasticity data, as described in Chapter 3. Simple alignment methods can be implemented to reduce the errors, where the user does not rely on an axis labeled on each individual optic as the reference, but relies on one optic as the reference optic to base all of the alignment. The objective is to set the axes of these optics such that transmitted light is extinguished when the optics are properly aligned. Either a CCD or a photodiode may be used to monitor the transmitted light. Firstly, the first polarizer alignment must be fixed as the reference axis for the other optics. Ideally, this first

polarizer is also aligned with the coordinates of the specimen, which may be achieved by assuring that light is extinguished for a polarized crystal at the specimen plane with the first polarizer at $\pi/2$ radians from the polarization of the crystal. Secondly, the second polarizer alignment is set to $\pi/2$ radians from the first polarizer to extinguish transmitted light. Thirdly, the $\lambda/4$ plates, when between the two crossed polarizers, should have light extinction when aligned with either of the two polarization optics. Fourthly, a loaded test specimen should be used to test the alignment for both photoelasticity and CGS by checking for the phase modulation errors in the wrapped φ_{sum} for CGS and in the wrapped α for photoelasticity. Small alignment adjustments can be made before a full experiment is conducted, which can especially reduce the errors in the isoclinic angle. In the proof of concept studies for the polycarbonate and Homalite-100 specimens presented in this thesis, the first three steps were taken for alignment, but not the fourth step, which can correct for the last degree or two of misalignment. A small $\pi/90$ radians misalignment in just the first $\lambda/4$ plate, such as those modeled in Sections 3.3.2.2, 3.3.2.3, and 4.2.4.2, can lead to significant errors (if not corrected). This systematic alignment should minimize phase modulation in both techniques.

If a non-polarizing beamsplitter is used for this experimental method, purchasing one with $T_x = T_y$ and $R_x = R_y$ coefficients eliminates the errors for the data. If this is not possible or prohibitively expensive, obtaining these coefficients from the manufacturer will help to at least quantify the error. These coefficients may easily be incorporated into the phase-shifting solution as detailed in Section 3.2.1, but incorporation of these coefficients into CGS requires rederiving the equations of intensity from Chapter 2. Another option is to perform CGS on the beam after the beamsplitter that has transmission/reflectance coefficients that are better matched and perform photoelasticity with the other beam since the transmission/reflectance coefficients can be incorporated for photoelasticity.

5.2.2 Isoclinic Angle Determination

If rotational alignment of the polarization optics is not precise, then the analysis program should be able to correct the errors in the wrapped isoclinic angle. The current manual methodology is sufficient for these photoelastic cases since the form of α is expected to be slowly varying for most

of the field, except in cases like that near the crack plane in Mode I–dominant fracture. Before extending this method to materials where the isoclinic angle may be more complicated or even have a new relationship to stresses due to the generalization of photoelasticity to anisotropic crystals, a robust algorithm should be developed for correcting for errors in the wrapped α. Some helpful features of this algorithm would be (i) removal of the errors even in the presence of other experimental errors, in the spirit of the quality-guided PCG unwrapping algorithm, (ii) user's ability to define masks to prevent removal of physical boundaries, and (iii) user's ability to define regions of high and low confidence based on metrics detailed in Section 3.2.4.1.

5.2.3   CGS Phase Relationship with Stress

The error associated with assuming the CGS phases are related to the first derivatives of $\sigma_1 + \sigma_2$, first characterized by Bruck and Rosakis (1992, 1993) for Mode I fracture and here in Chapter 4, requires revisiting to provide a full picture for applications of mixed-mode fracture. As indicated in the present study, small mode-mixity μ_{SIF} from -0.010 to 0.020 demonstrated increased error over the field of view as mode-mixity increased, particularly for the shearing direction related to the x derivative of $\sigma_1 + \sigma_2$. Since Mason et al. (1992) established that CGS can be applied to dynamic mixed-mode applications using the x derivative with good K_{II}/K_I measurement agreement with theory and finite elements, then possibly CGS studies with higher mode-mixity have acceptable error. Determining if these conjectures are true requires careful theoretical and experimental study with a wide range mode-mixity.

Beyond dealing with the error of the derivative assumption, another possible route to extracting $\sigma_1 + \sigma_2$ from CGS data is to treat the CGS phase precisely as a finite difference, where

$$\varphi_{sum} = \frac{2\pi C h}{\lambda}[s(x + d_{shear}/2, y) - s(x - d_{shear}/2, y)] \qquad (5.1)$$

where $s = (\sigma_1 + \sigma_2)$. Written in terms of pixel location, for $L = d_{shear}/[2 * \text{pixel resolution}]$, the

CGS phase for the i-shearing direction is

$$[\varphi_{sum}^i]_{i,j} = \frac{2\pi Ch}{\lambda}[s_{i+L,j} - s_{i-L,j}]. \tag{5.2}$$

This type of finite difference problem is a well defined concept in numerical methods called staggered grids. Taking the data from both shearing directions allows for an inverse determination of $\sigma_1 + \sigma_2$, still assuming that the "integration" of the finite difference data is a discrete Poisson equation. This change only requires a modification to the current Poisson equation in Equation (3.12) by changing the assumed resolution of the "derivative" from one pixel to the actual finite difference spacing of $2L$, such that

$$
\begin{aligned}
(s_{i+2L,j} - 2s_{i,j} + s_{i-2L,j}) &+ (s_{i,j+2L} - 2s_{i,j} + s_{i,j-2L}) \\
&= \left[\left(\frac{\varphi_{sum}^i \lambda}{2\pi Ch}\right)_{i+L,j} - \left(\frac{\varphi_{sum}^i \lambda}{2\pi Ch}\right)_{i-L,j}\right](2L) \\
&\quad + \left[\left(\frac{\varphi_{sum}^j \lambda}{2\pi Ch}\right)_{i,j+L} - \left(\frac{\varphi_{sum}^j \lambda}{2\pi Ch}\right)_{i,j-L}\right](2L), \tag{5.3}
\end{aligned}
$$

where φ_{sum}^i is the CGS phase in the i-shearing direction and φ_{sum}^j is the CGS phase in the j-shearing direction. Solving this Poisson equation would require a new algorithm because the PCG algorithm used in the current method is based on pixel distance as the finite difference spacing. This method is a more direct way of determining $\sigma_1 + \sigma_2$ without requiring the derivative assumption, which introduces the ϵ error discussed before. Previous fracture studies using CGS did not attempt to integrate the data to determine $\sigma_1 + \sigma_2$ as in this study, but instead use the CGS phases directly to make physical observations. The key to their studies is making the derivative assumption, giving the interference phase physical meaning as opposed to a finite difference that is difficult to physically interpret. The use of CGS to extract $\sigma_1 + \sigma_2$ lifts this need for a physical interpretation of the finite difference and in turn can eliminate the error associated with the derivative assumption.

5.3   Extensions of Method to Crystalline Materials

5.3.1   Development of Anisotropic Fracture Criteria

The phase-shifting CGS-photoelasticity experimental method has been demonstrated in stress-induced birefringent materials that are otherwise isotropic, but the method cannot in general be used for other types of materials in its current form. In order to extend the experimental method, the following requirements for both the materials of interest and the method must be met:

1. The crystalline materials must be transparent and have a detectable photoelastic (stress-optic) effect.

2. The appropriate photoelasticity governing equations are determined using the generalized theory for photoelasticity in crystals (Narasimhamurty, 1981). The basics of this theory are derived in Appendix C.

3. The governing equations for CGS in crystalline materials must be developed, utilizing the generalized theory for photoelasticity and elasticity in crystals.

With these requirements met, appropriate modifications to the optical setup and analysis may be developed to accommodate the new theory, if necessary. A full study of optically active ferroelectric crystals may be started once this method is extended to general crystals. These ferroelectrics have an additional challenge of spontaneous birefringence, discussed below.

Given the development of this hybrid method for transparent crystals with a detectable stress-optic effect, evaluation of full-field stresses around a crack may allow for development of general anisotropic fracture criteria. Experiments using crystals with different symmetries acting as model anisotropic materials may quanitify how anisotropic fracture depends on crystal symmetry in addition to local stresses and energy-related values ($\sigma_{\theta\theta}$, K_I, K_{II}, and G). For example, a crystal with cubic symmetry may require different fracture criteria than a crystal with monoclinic symmetry. Full-field stress determinination allows for calculation of the local crack tip stresses and energy-related values so that different fracture criteria depending on θ (max-K_I, $K_{II} = 0$, max-$\sigma_{\theta\theta}$, and

max-G) may be evaluated for each crystal symmetry. Determining fracture criteria for crystals that are not active materials can serve as a good foundation for studying active materials that bring an added level of complexity beyond crystal anisotropy.

5.3.2 Preliminary Investigation for Application to Ferroelectrics

Before investing in a full study of ferroelectric materials using this CGS-photoelasticity experimental method, a logical first step is to blindly attempt to image a loaded single-crystal ferroelectric using the current experimental method. The ferroelectric crystal used for this preliminary investigation is barium titanate ($BaTiO_3$), which is a tetragonal crystal at room temperature, meaning the crystal structure is a square base with side length a and perpendicular rectangular sides with long side length c (Jona and Shirane, 1993). $BaTiO_3$ has a large c/a ratio of 1.06, which leads to 6% actuation strain when electromechanically loaded. $BaTiO_3$ is of particular interest for photonic microdevices due to its high electro-optic nonlinearity. The spontaneous birefringence without stress is $\Delta n = -0.072$ with $n_o = 2.432$ (Yariv and Yeh, 2007), which implies in a stressed $BaTiO_3$ crystal, the birefringence viewed by an optical method is due to both the spontaneous birefringence and the stress-induced birefringence. The basis of the use of photoelasticity to study ferroelectric materials is if the crystal has a large enough stress-induced birefringence that can be detected, especially when coupled with a spontaneous birefringence.

The crystal used here is a single crystal with <001> orientation, meaning the long axis is aligned with thickness of the crystal and with the optical axis of the light source (z axis). The crystal then has two possible polarization states, along the $+z$ or $-z$ axis; a region with the same polarization state is called a domain. The specimen is 5 mm × 5 mm and 1.01 mm thick. The loading configuration is a distributed load by a wedge on the side of the crystal, which is clamped on the opposite side by a specimen holder. The image field of view is 4.52 mm × 4.52 mm with 4.5 μm resolution. The light source is a He-Ne laser with $\lambda = 632.8$ nm. The CGS parameters are the following: $p = 1$ mm/40, $\tilde{\Delta} = 8\ .87$ mm, and $d_{shear} = 226\ \mu$m. The phase-shifting methods in terms of the procedure of changing the optics are the same as for the photoelastic materials, introduced in Chapters 2

and 3, but the physical interpretations of the interference patterns are not necessarily applicable to ferroelectrics. All three possible polarization configurations for CGS are employed.

Figure 5.1 shows the six photoelasticity images from the six combinations of polarization optic angles in Table 3.1. The images that pertain only to the isochromatic phase in photoelastic materials, I_1 and I_2, appear more complicated than usual, with breaks in continuity of the fringes along vertical lines. These vertical lines are likely 180° domain walls, which are the boundaries between domains with polarization state that are 180° different. Since the stresses in the crystal should be continuous across these domain walls, the breaks in the interference fringes at these domain walls likely implies that two adjacent domains affect the Δn differently, modulating the stress-related Δn term. The other four images that usually pertain to both the isochromatic phase and the isoclinic angle do appear different from each other and from I_1 and I_2. I_4 and I_6 are similar to I_1 and I_2 in structure, but I_3 and I_5 only exhibit faint weak fringes and a crack in the crystal emanating from the load application point. The presence of the crack appears to further complicate the interference patterns.

The next step in the experimental method is to try to determine the isoclinic angle and the isochromatic phase using Equations 3.3 and 3.4. Using the BaTiO$_3$ experimental images I_1 through I_6 as if they originated from an ordinary photoelastic material yields the "wrapped isoclinic angle" in Figure 5.2(a), which is then used without unwrapping to give an "ambiguous wrapped isochromatic phase" in Figure 5.2(b). These wrapped phases do exhibit behavior consistent with the isoclinic angle and isochromatic phase. Figure 5.2(a) has many phase discontinuities reminiscent of the false phase discontinuities in α for the photoelastic materials that appear to correspond to the sine of the phase in Figure 5.2(b) going to zero. Otherwise, this α-like phase does not have phase discontinuities except near the crack. Ignoring the modulation by the δ-like phase, the α-like phase has mostly values close to zero, implying that the principal axes of the crystal are aligned with the Cartesian axes. Since this is a crystal, the principal axes will align with the crystal structure, so an α-like quantity in a tetragonal crystal is likely to be close to zero or $\pi/2$. The wrapped δ-like phase in Figure 5.2(b) has breaks in the phase discontinuities at the domain walls, illustrating the effect of the spontaneous birefringence of different domains on the Δn. The wrapped δ-like phase also

has what appears to be ambiguous data near the crack, possibly due to the regions in the α-like phase that require unwrapping. These conjectures require further investigation to determine the physical meaning behind these phases and to determine if these are even the appropriate quantities to consider. The interference patterns from the photoelasticity setup, though without quantified relationships to stresses, do exhibit some change in refractive index related to stresses that is large enough to detect using polarization optics. These images give hope to the idea that photoelasticity can be used to investigate stresses in ferroelectric crystals.

The images from the phase-shifting vertical and horizontal shearing CGS for all three polarization configurations introduced in Chapter 2 are presented in Figure 5.3. These images are complicated for two main reasons: (i) the polarization of different domains lead to discontinuous Δn, which then produce discontinuous CGS phases, and (ii) the finite shearing distance leads to interference of ΔS (optical path difference) from parts of the crystal that may have different domains, which can also lead to discontinuous CGS phases. In this case, the least complicated images come from the pure $E_y\hat{j}$ input, which may have some polarization significance. Having acquired four phase-shifted images for each case in Figure 5.3, the wrapped phase can be determined using the standard arctan() formula that gives a range from $(-\pi/2, \pi/2]$, as shown in Figure 5.4. These wrapped phases have the discontinuous fringes at the domain walls, but the phase appears either continuous or has the appropriate π phase discontinuity expected from wrapped CGS phases in vertical strips, which implies that these phases could be unwrapped inside these vertical strips. The obvious first steps are to determine the ΔS for a stresses ferroelectric and then determine the intensity relationship for these interference patterns, because from first glance, interpreting these CGS images is nontrivial. Fortunately, the stress-related optical effects and other optical effects in these ferroelectrics are well characterized, so determination of the intensities is only a matter of careful analysis.

5.4 Conclusions

The future research for this CGS-photoelasticity experimental method pertains to two main avenues, improving the current method and then extending it to investigate fracture in crystalline materi-

als. Errors related to misalignment of optics and to the non-polarizing beamsplitter may easily be mitigated by careful alignment procedures outlined above and by characterizing the quality of the optics. Also, a robust algorithm should be developed to reduce errors due to corrections to the wrapped isoclinic angle. To eliminate the inherent error in assuming that the CGS phase is related to the derivative of $\sigma_1 + \sigma_2$, the CGS phase is to be treated as a finite difference, and then the vertical and horizontal phase data are integrated using a new form of the discrete Poisson equation based on staggered grids. The extension of the experimental method to crystalline materials depends mainly on a detectable photoelastic effect from the crystal and on extensive analysis on the interference patterns in the individual experimental techniques. A preliminary investigation of the ferroelectric $BaTiO_3$ demonstrates that this crystal has a detectable photoelastic effect, but this effect is confounded by the spontaneous polarization; further analysis is required to determine the physical meaning of interference patterns from both photoelasticity and CGS for this ferroelectric.
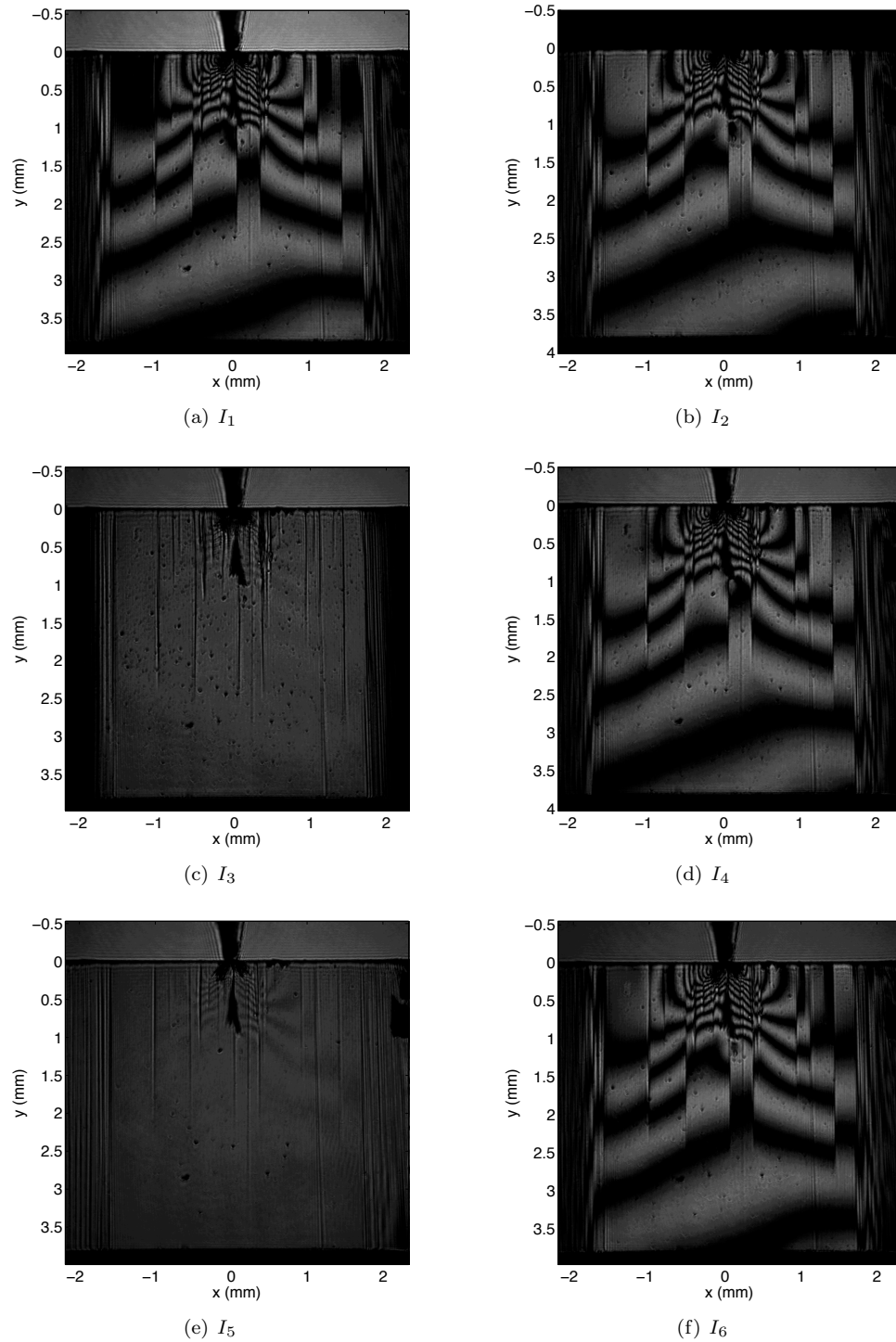
(a) I_1

(b) I_2

(c) I_3

(d) I_4

(e) I_5

(f) I_6

Figure 5.1: Experimental images from six-step phase-shifting photoelasticity for a side-loaded BaTiO$_3$ single crystal

(a) I_1

(b) I_2
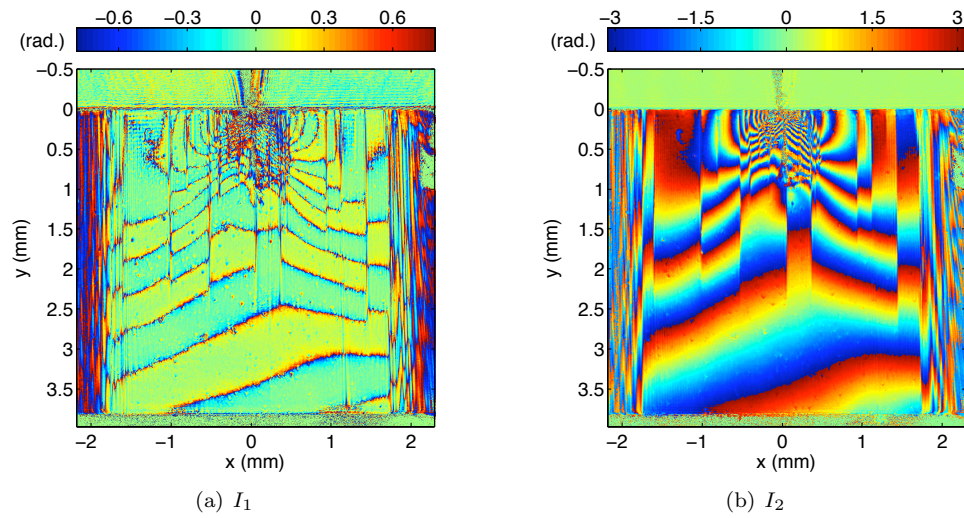
Figure 5.2: Experimental wrapped phases from six-step phase-shifting photoelasticity for a side-loaded BaTiO$_3$ single crystal

(a) Vertical I_1 from pure $E_x\hat{\imath}$

(b) Horizontal I_1 from pure $E_x\hat{\imath}$

(c) Vertical I_1 from pure $E_y\hat{\jmath}$

(d) Horizontal I_1 from pure $E_y\hat{\jmath}$

(e) Vertical I_1 from circular polarization

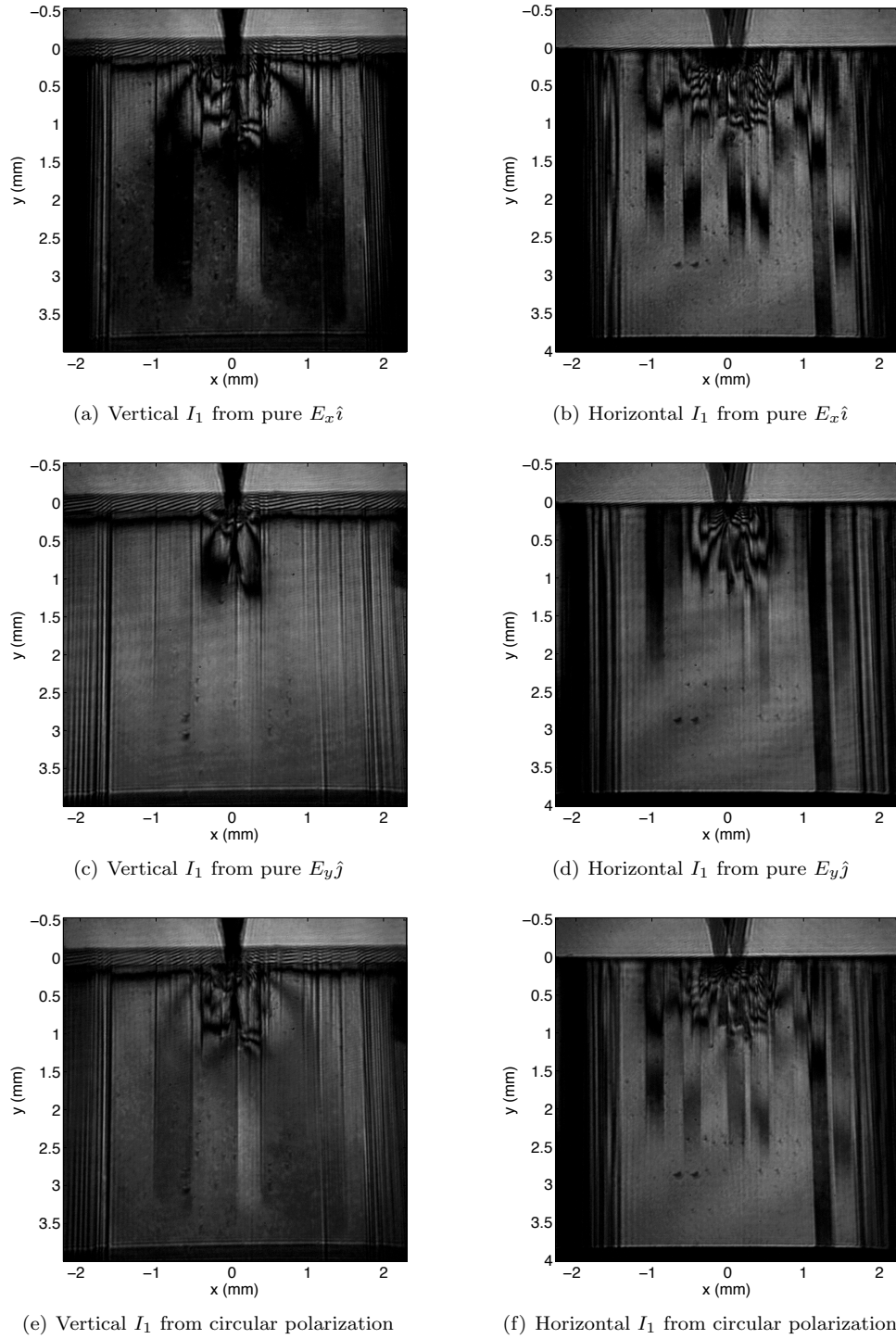(f) Horizontal I_1 from circular polarization

Figure 5.3: Experimental images I_1 from the three polarization configurations for vertical and horizontal shearing directions for a side-loaded BaTiO$_3$ single crystal

(a) Vertical I_1 from pure $E_x\hat{\imath}$

(b) Horizontal I_1 from pure $E_x\hat{\imath}$

(c) Vertical I_1 from pure $E_y\hat{\jmath}$

(d) Horizontal I_1 from pure $E_y\hat{\jmath}$

(e) Vertical I_1 from circular polarization

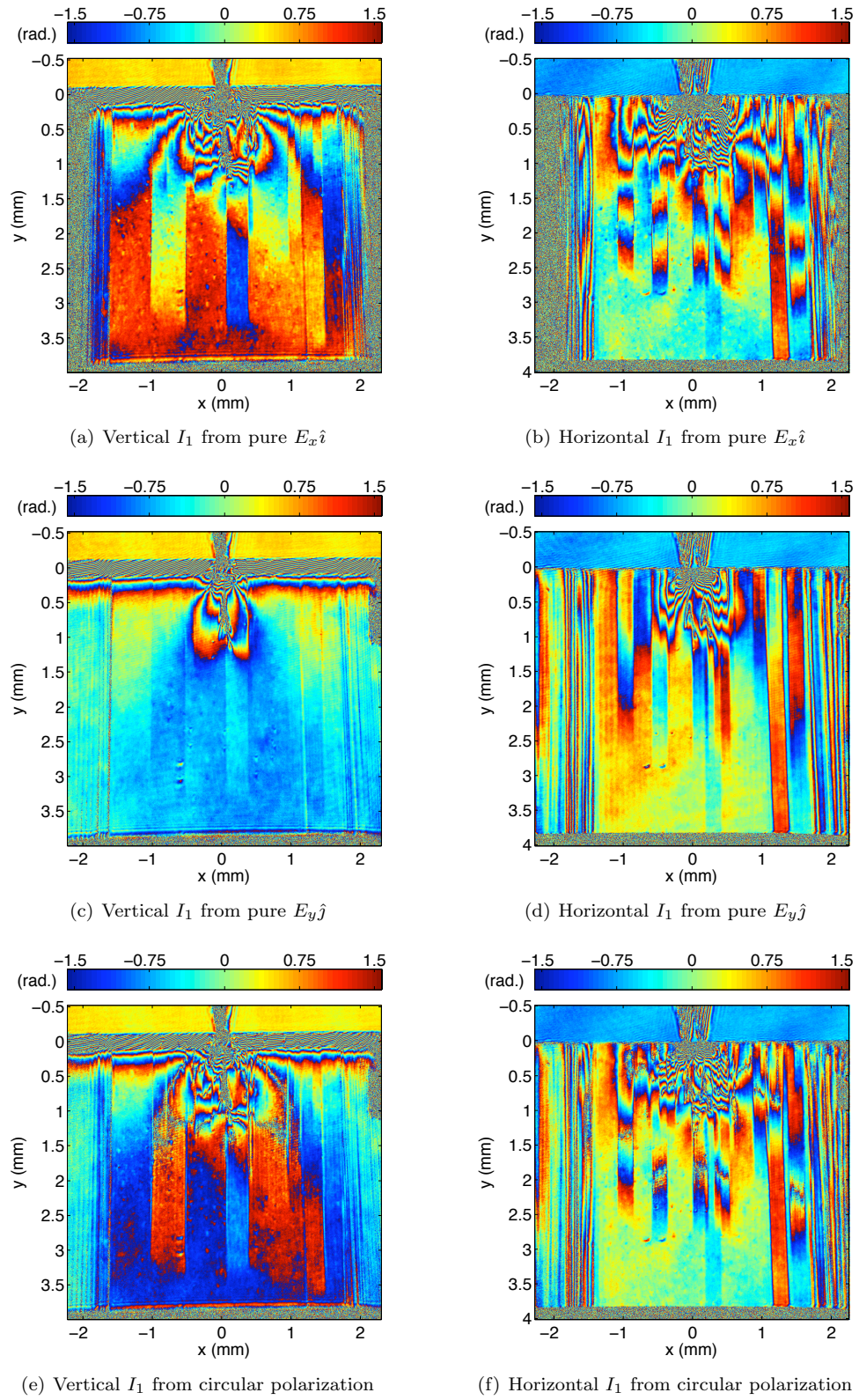(f) Horizontal I_1 from circular polarization

Figure 5.4: Experimental wrapped phases from the three polarization configurations for vertical and horizontal shearing directions for a side-loaded BaTiO$_3$ single crystal